Available online at www.sciencedirect.com
SCIENCE DIRECT®
Journal of Nuclear Materials 348 (2006) 148–164
journal of nuclear materials
www.elsevier.com/locate/jnucmat

The effect of dose rate on the response of austenitic stainless steels to neutron radiation

T.R. Allen [a,*], J.I. Cole [b], C.L. Trybus [b], D.L. Porter [b], H. Tsai [c], F. Garner [d], E.A. Kenik [e], T. Yoshitake [f], Joji Ohta [g]

[a] University of Wisconsin, 1500 Engineering Drive, Madison, WI 53706, USA
[b] Argonne National Laboratory, P.O. Box 2528, Idaho Falls, ID 83403, USA
[c] Argonne National Laboratory, 9077 Cass Ave, Argonne, IL 60439, USA
[d] Pacific Northwest National Laboratory, P.O. Box 999, Richland, WA 99352, USA
[e] Oak Ridge National Laboratory, P.O. Box 2008, Oak Ridge, TN 37831, USA
[f] Japan Nuclear Cycle Development Institute, Ibaraki 311-1393, Japan
[g] Central Research Institute of Electric Power Institute, Tokyo 201-8511, Japan

Received 22 February 2005; accepted 13 September 2005

Abstract

Depending on reactor design and component location, austenitic stainless steels may experience significantly different irradiation dose rates in the same reactor. Understanding the effect of dose rate on radiation performance is important to predicting component lifetime. This study examined the effect of dose rate on swelling, grain boundary segregation, and tensile properties in austenitic stainless steels through the examination of components retrieved from the Experimental Breeder Reactor-II (EBR-II) following its shutdown. Annealed 304 stainless steel, stress-relieved 304 stainless steel, 12% cold-worked 316 stainless steel, and 20% cold-worked 316 stainless steel were irradiated over a dose range of 1–56 dpa at temperatures from 371 to 440 °C and dose rates from 0.5 to 5.8×10^{-7} dpa/s. Density and tensile properties were measured for 304 and 316 stainless steel. Changes in grain boundary composition were examined for 304 stainless steel. Swelling appears to increase at lower dose rates in both 304 and 316 stainless steel, although the effect was not always statistically significant. Grain boundary segregation also appears to increase at lower dose rate in 304 stainless steel. For the range of dose rates examined, no measurable dose rate effect on tensile properties was noted for any of the steels.

1. Introduction

For existing light-water reactors (LWRs) and some Generation IV concepts, many core components have been or will be constructed from austenitic stainless steels [1,2]. Depending on the specific core design and the location of the component in the core, the damage rate experienced can vary by orders of magnitude. For example, a cladding material in a supercritical water-cooled reactor will experience a damage rate approximately two orders of magnitude greater than that of a mid-core

* Corresponding author. Tel.: +1 608 265 4083; fax: +1 608 263 7451.
E-mail address: allen@engr.wisc.edu (T.R. Allen).

0022-3115/$ - see front matter
doi:10.1016/j.jnucmat.2005.09.011

baffle-former junction in a pressurized water reactor (PWR) of currently operating design.

From previous fast reactor development programs, a significant database exists for the properties of austenitic stainless steels at high dose rates ($\sim 1 \times 10^6$ dpa/s) and temperatures from 370 to 550 °C. An earlier review by Garner [3] showed that even in the fast reactor range of displacement rates there was an indication that the duration of the transient regime of swelling in austenitic steels was dependent on the dpa rate, leading to increases in swelling as the dpa rate decreased. This review also showed that there was a limited amount of data showing that mechanical properties of austenitic steels might be dose rate-sensitive. Later papers by Garner predicted that the lower swelling rate encountered in PWRs might actually increase the swelling at a given dose [4,5]. A group of datasets have been published recently that examine the swelling behavior of various Western and Russian austenitic steels at lower LWR-relevant temperatures and especially lower dose rates characteristic of Western PWRs and Russian VVERs [6–17]. These papers all have the common theme that the evolution of void microstructure appears to be strongly dose rate-sensitive, with swelling increasing at lower dpa rates.

Fig. 1 shows the typical mid-core dose rate distribution as a function of radial position for EBR-II. Note that the dose rates experienced by reflector components in rows 8–14 are approximately an order of magnitude lower than those of typical EBR-II test positions in the inner core region rows 1–4. Comparing data taken from irradiated reflector components with data taken from components irradiated in inner test locations therefore allows examination of dose rate effects. Examining components taken within the reflector row region, where the large damage rate gradient exists, allows additional determination of dose rate effects.

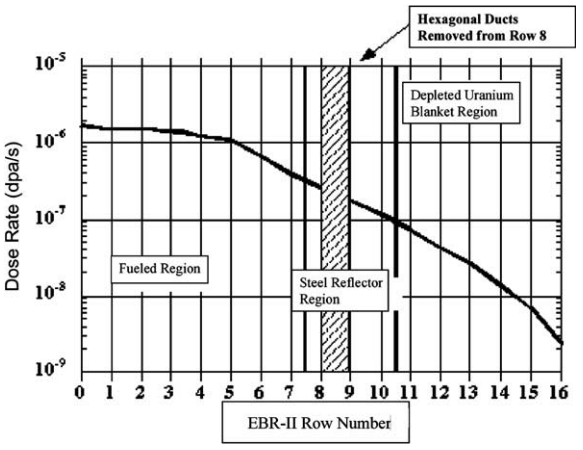

Fig. 1. Dose rate as a function of radial core position in EBR-II at core centerline.

As part of the Experimental Breeder Reactor (EBR-II) reactor materials surveillance (SURV) program [18–22], test samples of AISI 304 stainless steel were placed into EBR-II in 1965, with the intention of determining changes in microstructure, corrosion, and mechanical properties due to irradiation and thermal aging. The peak displacement rate for the materials in the SURV subassemblies, located in row 12, was approximately 6.5×10^{-8} dpa/s. This displacement rate is about one-and-a-half orders of magnitude lower than used in a typical accelerated reactor materials test but within the range of displacement rates experienced by commercial light-water reactor (LWR) core components [4,5,23].

Following shutdown of the EBR-II reactor, surveillance test samples constructed of 304 stainless steel were retrieved to determine the effect of low dose rate irradiation on mechanical properties and microstructure. In addition to the SURV specimens, a large quantity of hexagonal duct (also referred to in this paper as hex can) material, made of 304 and 316 stainless steel with a thickness of approximately 1 mm, was retrieved from rows 8 to 14 of the reflector region. These components were irradiated over a dose range of 1–56 dpa at temperatures from 371 to 440 °C and dose rates from 0.5 to 5.8×10^{-7} dpa/s. Additionally, data from an inner row core thimble irradiated up to 80 dpa at temperatures from 371 to 440 °C has been included in the examination of swelling properties of 12% CW 316.

The effect of dose rate on swelling, grain boundary segregation, and tensile properties in 304 and 316 austenitic stainless steels, determined through the examination of material retrieved from the Experimental Breeder Reactor-II (EBR-II), is reported in this work.

2. Experiment

Table 1 lists the origin of the samples used in this study. Annealed 304 stainless steel samples were available from hex ducts (Fig. 2) irradiated in rows 10 and 14 of EBR-II. The two hex ducts were from different lots and therefore had slightly different compositions. The row 10 hex duct was in a single

Table 1
Summary of sample material origin

	304	12% CW 316	20% CW 316
Density	Hex can row 10 (annealed) Hex can row 14 (annealed) SURV rows 4, 12 (annealed) SURV row 12 (stress relieved)	Hex can rows 8 and 9 Control-rod thimble (CRTH 31)-row 5	Hex can row 8
Microstructure/microchemistry	Hex can row 10 (annealed) Hex can row 14 (annealed) SURV rows 4, 12 (annealed)	Hex can rows 8 and 9	Hex can row 8
Tensile	SURV rows 4, 12 (annealed)	Hex can rows 8 and 9	Hex can row 8

Rows 10 and 14 hex duct 304 from different lots of steel.
Rows 4 and 12 SURV annealed material from a single lot of steel.
Row 12 stress-relieved SURV material from a different lot than the row 4/12 annealed material.
Rows 8 and 9 12% CW 316 from same lot of steel.
Row 5 CRTH 316 from different lot of steel than row 8 and 9 hex ducts.

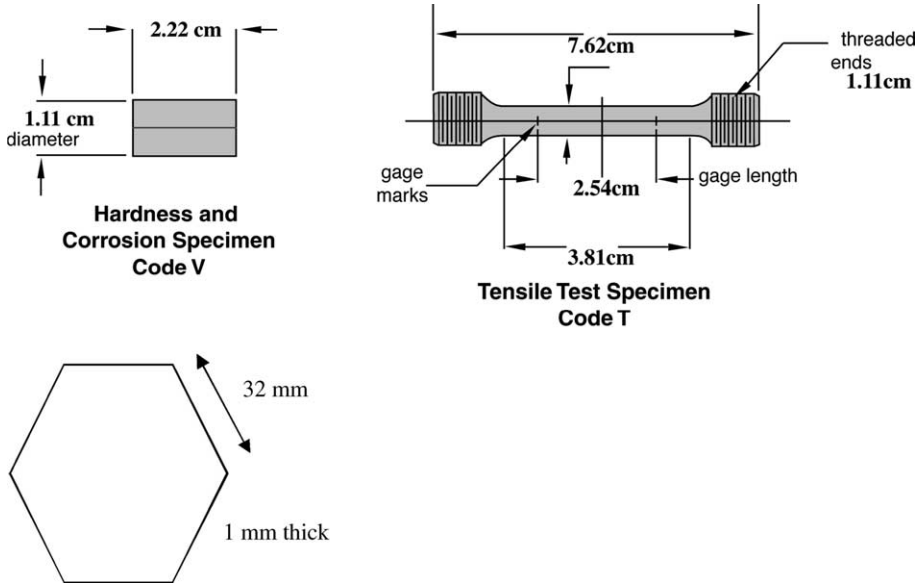

Fig. 2. Dimensions of surveillance (SURV) hardness specimen, SURV (round) tensile specimen, EBR-II hexagonal duct, and hex can (flat) tensile specimen.

location for the entire irradiation history. The row 14 hex duct started in row 8 for 2.4 dpa and then was moved to row 14 for an additional 7.6 dpa. Additional annealed 304 stainless steel was available from SURV specimens (Fig. 2) irradiated in rows 4 and 12 of EBR-II. A second set of 304 SURV specimens irradiated in row 12 were stress relieved, but not fully annealed. All SURV specimens remained in a single location of the reactor for their entire irradiation history.

Within the EBR-II surveillance program, two different lots of 304, two different processing histories (stress relieved and annealed), and two different core locations (rows 4 and 12) were investigated [24]. Stress-relieved surveillance samples were 20% cold-worked with a stress-relief 2 h heat treatment of 468–496 °C following machining. The annealed 304 SURV specimens were the same used in constructing the EBR-II cover plate. Similar to the hex cans, displacement rates varied along the length of each SURV subassembly leading to samples with varying temperature, dose, and dose rate, depending on their radial and axial position within the test assembly.

Table 2
Irradiation conditions

Material	Temperature (°C)	Peak dose (dpa)	Dose rate (dpa/s)
Annealed 304 hex can	371–400	25	$0.02–1.0\times10^{-7}$
Stress-relieved 304 SURV row 12	371–400	20	$0.3–6.5\times10^{-8}$
Annealed 304 row 4	371–400	11	$0.1–1.0\times10^{-6}$
Annealed 304 row 12	371–400	18	$0.3–6.5\times10^{-8}$
12% CW 316 hex can	371–460	56	$0.1–5.8\times10^{-7}$
12% CW 316 CRTH	371–460	80	$3.7–8.5\times10^{-7}$
20% CW 316 hex can	371–390	47	$0.8–3.5\times10^{-7}$

Cold-worked 316 stainless steel, both 12% and 20% cold-worked, was also available from hex cans irradiated in rows 8 and 9. The hex ducts from rows 8 and 9 were from the same lot and thus had identical compositions. Additionally, 12% cold-worked 316, available from a row 5 control rod thimble (CRTH) was also analyzed. The row 5 CRTH was of a different lot of steel than the row 8 and 9 hex ducts. Table 2 lists the irradiation conditions for each of the available sample materials.

Density measurements were performed on either slices from an existing SURV specimen or on 19 mm diameter coupons punched from hex ducts. Density was measured using a water immersion technique. For selected samples, void size distributions were measured using a JEOL 2010 transmission electron microscope.

Tensile samples were either irradiated as round tensile bars in the SURV program or were prepared from 1 mm thick hexagonal ducts using an electrical discharge machining (EDM) process. Fig. 2 shows the two tensile types employed. Tensile samples of annealed 304 stainless steel were taken from hex duct material irradiated at temperatures between 371 and 390 °C and were tested at 370 °C. Tensile samples of 12% cold-worked 316 were taken from similar hex duct material irradiated at temperatures between 371 and 441 °C and were tested at ~380 °C or ~430 °C. Tensile samples of 20% cold-worked 316 were also taken from hex duct material irradiated at temperatures between 371 and 385 °C and were tested at ~370 °C. For the 12% and 20% cold-worked 316 stainless steel, the tensile samples were made from the same ducts that were used to produce density samples.

Tensile tests were performed in air and took a few hours for a typical test. The strain rate for the 12% cold-worked samples was $1\times10^{-3}\,s^{-1}$. The strain rate for 20% cold-worked tensile tests was $4\times10^{-5}\,s^{-1}$ and was taken to match the strain rate of a tensile test on 20% CW 316 irradiated at high displacement rate performed in the 1970s. At these temperatures, the difference in strain rates between the 12% and 20% cold-worked tests is not expected to significantly change the measured mechanical properties [25].

Samples for microstructural and microchemical analysis were prepared from a selected subset of the density samples. Following immersion density measurement, a subset of the density disks were thinned in a hot cell to a thickness of about 250 μm by mounting and grinding, using standard metallographic sample preparation techniques. Three-millimeter TEM sample blanks were then punched from these thinned disks using a special mechanical punch developed for hot cell use. TEM sample blanks were electropolished at −30 °C using a 5% perchloric acid/95% methanol solution until they became electron-transparent. Grain boundary compositions were measured using a Phillips CM200 FEG-STEM with an EMiSPEC X-ray analysis system. Other microstructural characterization was performed using a JEOL 2010 transmission electron microscope. To perform defect density measurements, it was necessary to determine sample thickness in the analysis regions. This was accomplished using convergent beam electron diffraction (CBED) with an electron probe size on the order of 10–15 nm. Pixel intensity profiles across the scanned CBED disk image were used to measure fringe spacing. The spacings were then converted to a thickness value as described in Ref. [64]. Both magnification and camera length were calibrated on the TEM prior to making quantitative measurements.

3. Results and discussion

3.1. Swelling in 304 stainless steel

Fig. 3 presents two sets of density data on 304 stainless steel. The first set is swelling data for

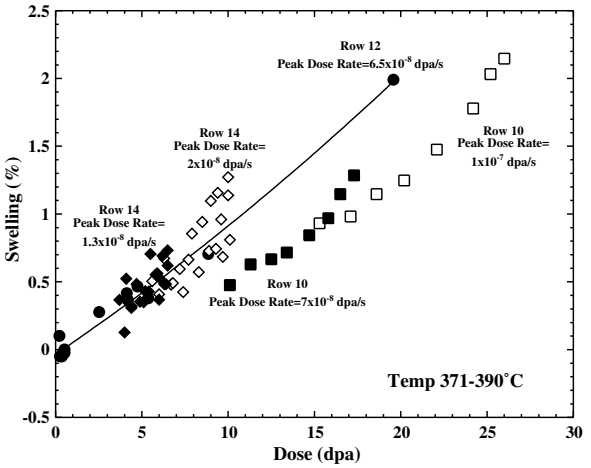

Fig. 3. Swelling from 304 stainless steel irradiated at various dose rates.

19 mm diameter disks taken from hexagonal cans irradiated in rows 10 and 14 of EBR-II. The larger the row number, the lower the average dose rate. The data on these two assemblies are a subset of a larger data set from five subassemblies now being published by Garner [26]. Because of the large dose rate gradient in the outer rows of EBR-II (Fig. 1), samples taken from the inboard hex can face (closer to the center of the core) have a significantly higher average displacement rate than samples taken from the outboard face of the hex duct. The samples from row 12 are stress-relieved 304 samples from the EBR-II surveillance program (Fig. 2).

Samples in a set of data from a given row were taken from different axial locations along the hex duct. Therefore, in Fig. 3 for samples taken from a single can or from the SURV assembly, the dose rate is different at each dose and there are differences in temperature also. At a given elevation on the hex duct the temperatures on each face of the can are always within 3 °C of each other. Dose rate effects are therefore examined by comparing the trends of data taken from different hex can faces.

Following a transient period, a 1%/dpa terminal swelling rate is eventually expected in all austenitic stainless steels at relatively high dose rates, as demonstrated by Garner and coworkers [3,26–28]. This behavior has been observed at high exposure in annealed 304 as well [29]. None of the data in Fig. 3 show such high swelling rates. Therefore these data all reside in the transient regime and have not yet reached steady-state swelling. Fig. 3 shows that, for a fixed dose, the swelling is always larger for samples irradiated at lower dose rate. Additionally, for a fixed dose, the rate of swelling is larger for samples irradiated at lower dose rate. For a fixed dose, the samples irradiated at lower dose rate are closer to the terminal 1%/dpa swelling rate expected in austenitic stainless steels. In other words, the swelling transient, the dose required to achieve a 1%/dpa swelling rate, is shorter for samples irradiated at lower dose rate. The high dose rate side of the row 10 hex duct (peak dose rate 1×10^{-7} dpa/s, open squares) appears to have the longest transient while the low dose rate side of the row 14 hex duct (peak dose rate 1.3×10^{-8} dpa/s, solid diamonds) appears to have the shortest transient. As might be expected, the density data from the row 12 SURV specimens appear to fall between the data from rows 10 and 14.

Each set of data points presented with the same symbol comes from samples taken along the same face of a hexagonal duct. Therefore, the temperature and dose rate are different for each data point since the temperature increases from the bottom to the top of the duct and the dose rate is largest at the core centerline. The dose rate and temperature change from one radial position (for example row 10) to another radial position (for example row 14) can be described by a fixed ratio, regardless of axial position. Therefore, comparing the trends of each curve provides information on displacement rate differences.

Unfortunately the density samples whose measurements are shown in Fig. 3 were taken from different lots of 304 stainless steel (Table 1). Compositions from the row 12 SURV samples were measured prior to irradiation. Unirradiated archive material exists for the row 10 hex duct, but not for the row 14 hex duct. Therefore, composition was determined from samples taken from both irradiated hex ducts (rows 10 and 14) using inductively coupled plasma–atomic emission spectroscopy (ICP–AES) for major elements and a LECO IR-412 Carbon Determinator for carbon. Table 3 provides the measured composition measurements (measured on irradiated samples) for each hex duct and the vendor specification chemistry (measured prior to irradiation) for the SURV samples. The concentrations of certain elements, such as phosphorous, known to have an important effect on swelling are not known. Even though a dose rate effect on swelling appears evident in Fig. 3, because the subassemblies and surveillance samples were fabricated from different lots of steel, differences in

Table 3
Bulk compositions determined from microchemistry samples (rows 10 and 14) and as supplied by the vendor (row 12 SURV)

Element	Row 10 hex duct (at.%)	Row 12 SURV (at.%)	Row 14 hex duct (at.%)
Cr	19.6	19.4	19.6
Ni	8.5	9.4	9.1
Fe	69.8	68.4	69.0
Mo	<0.02	0.12	0.07
Mn	0.82	0.90	1.01
C	0.4	0.4	0.5
Si	0.92	1.3	0.76

composition or grain size could exert some confounding influence on the interpretation of a dose rate-dependent duration of the transient regime. However, the data taken on two different faces (and thus different dose rates but identical composition) of the row 14 hex duct, shows a dose rate difference. Although compositional differences in the data presented here limit the ability to make a definitive conclusion on dose rate effects, to a much broader extent, Garner and coworkers have shown in a larger hex can data set that the dose rate effect can easily be seen in single heat comparisons [26].

The void size distributions for samples taken from specimens from rows 10, 12, and 14 are displayed in Fig. 4 for samples irradiated to comparable doses. Accompanying micrographs are seen in Fig. 5. The void size is the largest for those samples irradiated in row 14 at the lowest dose rate. The difference between the row 10 and 12 distributions is mainly due to differences in void density. Early in the transient, the differences appear to be due to void density differences while later in the transient, void size appears to become more critical. Very similar microscopy and density results have been previously presented by Bond and coworkers for annealed 304 from hex ducts in rows 8–10 and 14 of EBR-II [7].

As stated earlier the data in Fig. 4 come from different heats of material. The displacement rate effect on swelling in 304 stainless steel can also seen by comparing the microstructure of samples from the SURV heat irradiated in different rows. Fig. 6 displays the void size distributions for annealed 304 stainless steel irradiated in rows 12 and 4 for the SURV program. For a nearly constant dose, the low dose rate sample irradiated in row 12 shows larger swelling, a larger density of larger voids, than was observed in row 4.

The data on swelling in 304 stainless steel presented above indicate that for a fixed temperature

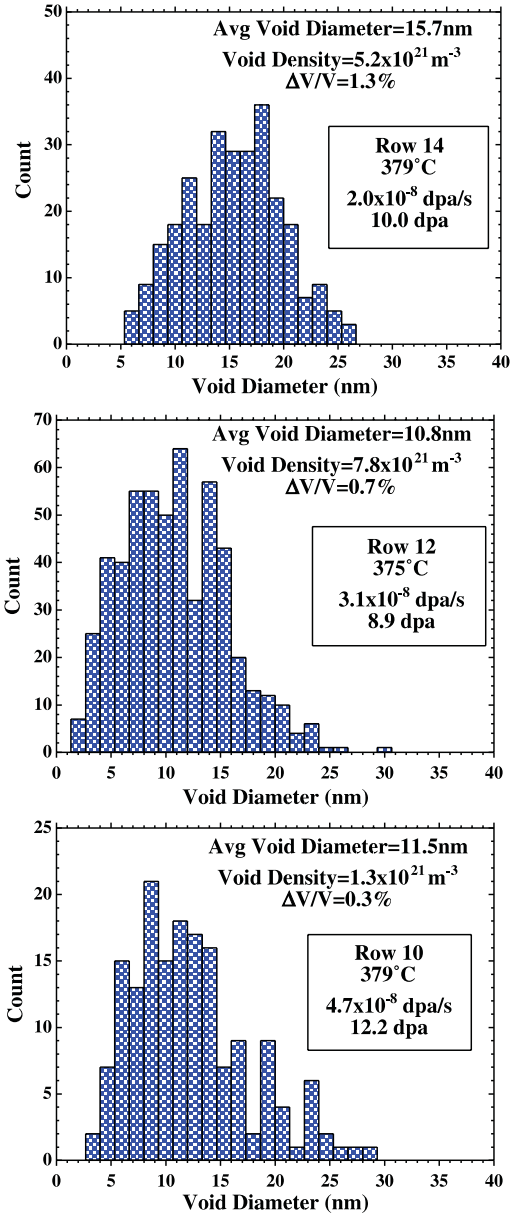

Fig. 4. Void size distributions for samples solution annealed 304 from rows 10, 12, and 14. $\Delta V/V$ is the swelling measured using immersion density. Rows 10 and 14 are hex can samples. Row 12 are SURV stress-relieved samples.

a decrease in dose rate leads to larger swelling at a given dose. This result is consistent with the earlier work of Porter and Hudman [30] that showed increases in displacement rate on 304 stainless steel irradiated at 390 °C at dose rates between 2×10^{-7} and 5×10^{-7} dpa/s led to a measurable reduction in swelling. Porter and Garner also showed that there was a strong synergistic effect of dpa rate

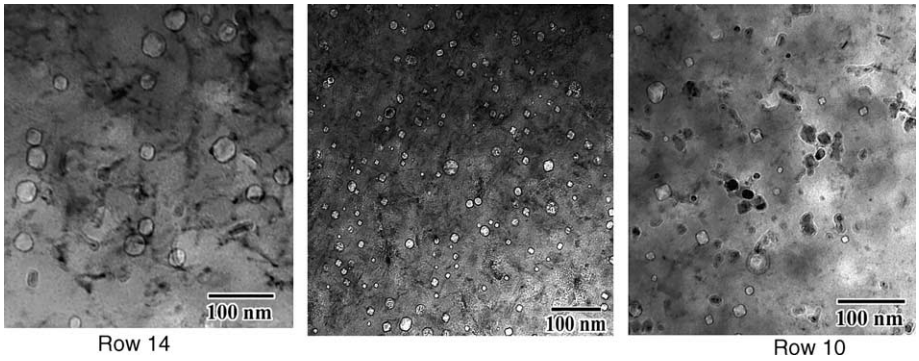

Fig. 5. Micrographs of voids in samples from rows 14, 12, and 10, corresponding to Fig. 4.

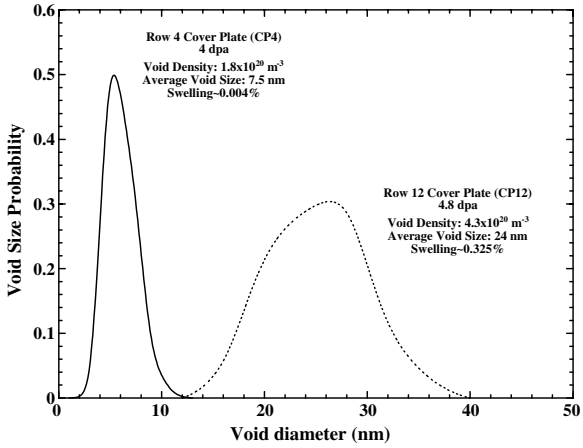

Fig. 6. Void size distribution for annealed 304 stainless steel, from the SURV cover plate, irradiated at different displacement rates in rows 4 and 12.

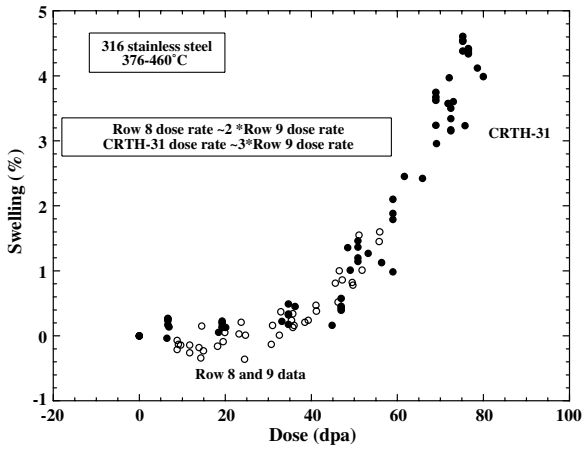

Fig. 7. Swelling as a function of dose for 12% cold-worked 316 stainless steel irradiated in rows 8 and 9 of EBR-II. CRTH-31 is a different heat than the row 8 and 9 hex cans.

and applied stress to determine the duration of the transient regime of swelling [31,32].

3.2. Swelling of cold-worked 316 stainless steel

The dose rate dependence of swelling was also investigated in 12% cold-worked 316 stainless steel. Density measurements from hex cans irradiated in rows 8 and 9 of EBR-II are compared in Fig. 7 with measurements from an EBR-II control rod thimble (designated CRTH-31) irradiated in row 5. The peak dose rate of 8.5×10^{-7} dpa/s in row 5 is about three times larger than the dose rate of row 9 hex duct and 1.5 times that of the row 8 hex can. Unfortunately, the thimble, which was irradiated to a peak dose of 80 dpa, was not from the same heat as the row 8 and 9 hex cans and its composition is not available. If we ignore this complication no discernible difference in density as a function of dose rate exists for CW 316 for a difference in dose rate of a factor of three.

At low dose, the samples from rows 8 and 9 undergo slight densification at low dose (≈20 dpa) before swelling becomes noticeable. Densification at low dose is somewhat less noticeable in the CRTH-31 samples. Once swelling becomes prevalent, however, no differences in swelling can be seen between the row 8, 9, and CRTH-31 samples.

Fig. 8 presents the swelling for six different pairs of 316 samples chosen to have similar irradiation temperature and dose, but differing in dose rate by a factor of two. The data are taken from the row 8 and 9 hex cans that are from the same material heat. In each case, the sample irradiated with the lower rate shows greater swelling. In all but one case, however, the difference in swelling is less than the experimental uncertainty. This figure indicates

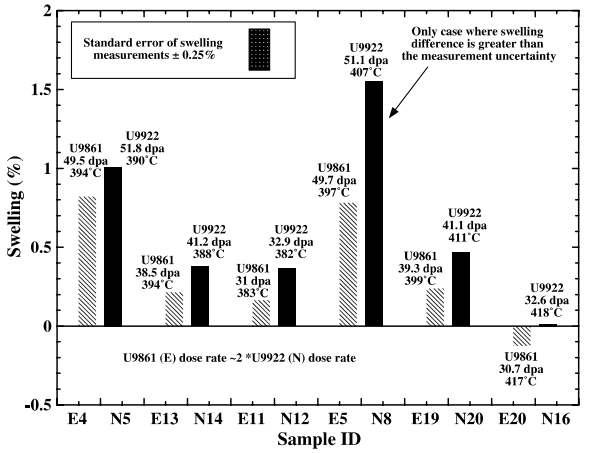

Fig. 8. Comparison of swelling in 12% CW 316 stainless steel for samples irradiated under similar conditions. E designates a row 8 (higher dose rate) sample while N designates a row 9 (lower dose rate) sample.

that swelling may vary with dose rate in 316, but a wider range of dose rates is needed to show a statistically significant effect.

The lack of a statistically significant dependence of swelling of AISI 316 on dose rate at 376–460 °C in this study may not preclude the role of dpa rate at other temperatures. Such behavior is consistent with the early measurements of Seran and Dupouy [33]. In their work, annealed 316 stainless steel was irradiated in the Rapsodie reactor at temperatures of 450, 500, and 550 °C. At 500 and 550 °C, a displacement rate effect on swelling was seen, with higher displacement rates leading to a longer period of transient swelling and less swelling for a fixed dose. The difference was smaller at 500 °C than at 550 °C. At 450 °C, no effect of displacement rate was discernible. Seran and Dupouy also showed that the dose rate effect on swelling could be observed at 562 °C in annealed 316 irradiated in Rapsodie and in CW 316 irradiated in Phenix at 590–610 °C [34]. Porter and Hudman showed that 5% cold-worked 316 stainless steel irradiated at 400 °C to 40 dpa in EBR-II between 4 and 6×10^{-7} dpa/s appear to swell more at lower dose rate [30]. The studies of Porter, Garner and Brager [35–39] indicated that the increased swelling was manifested as a shortened transient region and was associated with the removal of solutes from solution that tended to inhibit swelling. The dose rate effect on swelling is apparently dependent on both major element composition and temperature, with possible lot-to-lot variability associated with minor element composition and thermo-mechanical treatment.

3.3. Swelling: general conclusions

The swelling data presented in this report indicate that:

1. Swelling in annealed 304 stainless steel appears to always increase at a given temperature when the dpa rate decreases. Swelling in 316 seems also to be likewise sensitive to dpa rate but the differences at lower irradiation temperatures are not always statistically significant, reflecting primarily the lower amount of swelling compared to that produced in annealed 304 under comparable conditions.
2. The differences appear to be due to a dose rate-sensitive change in the transient period when void distributions are developing. Although not shown in this study, dose rate effects on swelling do not appear to affect the steady-state swelling rate of ~1%/dpa [63]. Recent studies by Okita and coworkers have shown that in simple model austenitic alloys, the primary influence of dpa rate is manifested in the duration of the transient regime of swelling, with the major effect of dpa rate operating on the loop and dislocation evolution, but the terminal steady-state rate is unaffected [43–46].

3.4. Grain boundary segregation in 304 stainless steel

As noted above, Porter, Garner, and Brager postulated that the precipitation-induced removal of certain solutes (Ni, Si, P) from 304 or 316 stainless steel decreased the transient regime of swelling [35–38]. Voids, once formed, also lead to significant segregation of nickel and rejection of chromium at their surfaces [39,40], while a smaller level of segregation can occur on sessile Frank loops [41,42]. Therefore, microchemical changes associated with voids, precipitates, and dislocation loops may be critical to overall microstructural development of irradiated alloys. The segregation mechanisms that produce this linkage between microstructure and microchemistry also operate at grain boundaries [42]. In particular there is concern that radiation-induced depletion of chromium at grain boundaries may make austenitic steels more susceptible to grain

boundary attack in water-cooled or lead alloy-cooled reactor systems.

Therefore the effect of dose rate on radiation-induced segregation at grain boundaries was investigated in 304 stainless steel, measuring chromium depletion, as well as nickel and silicon enrichment for samples irradiated in rows 10 (hex can), 12 (stress-relaxed SURV), and 14 (hex can) are shown in Fig. 9. These samples were prepared from density samples discussed in the previous section on swelling. As the displacement rate decreases, the amount of nickel enrichment and chromium depletion clearly increases. Even at half the dose, the row 14 sample has greater radiation-induced segregation (RIS) of Ni and Cr than that of the row 12 sample.

Theory predicts that radiation-induced grain boundary segregation depends on both temperature and dose rate. Fig. 10 presents model predictions for chromium depletion in Fe–20Cr–9Ni ternary alloy, that is similar to 304 stainless steel without minor solutes such as C, Mn, Si and P [47]. At temperatures in the range 379–389 °C, chromium depletion is predicted to increase with decreasing dose rate, in agreement with the data in Fig. 9.

However, our data concerning dose rate effects on grain boundary segregation cannot be considered to be a perfect single-variable experiment, especially with respect to composition. While Mo in 316 steels is usually rather large (~2%) the levels in 304 are traditionally small, as is the case in all three heats tested in this study (0.02–0.07–0.12%). Note that the row 12 and 14 samples have measurably larger molybdenum concentrations than the row 10 sample (see Table 3), which might have influenced

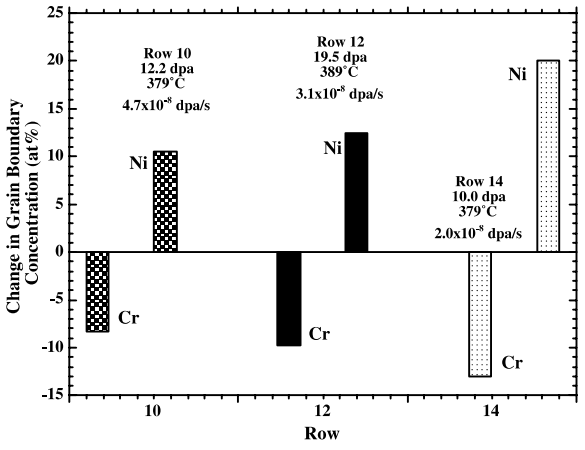

Fig. 9. Radiation-induced grain boundary segregation measured in 304 samples from rows 10, 12, and 14.

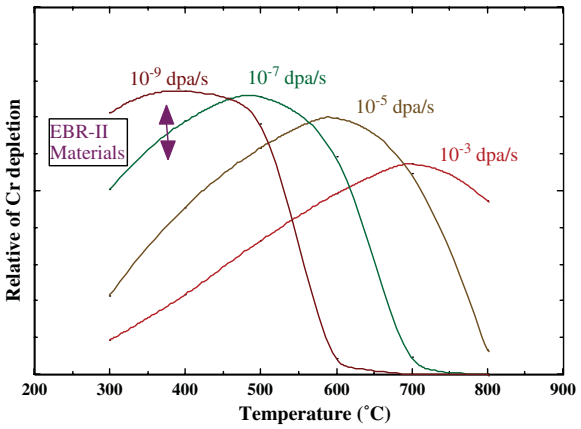

Fig. 10. Predicted relative chromium depletion as a function of temperature and dose rate in Fe–20Cr–9Ni [38].

the segregation of other elements. Molybdenum is known to influence the swelling, precipitation and diffusion behavior of austenitic steels [48] and therefore may influence the segregation at grain boundaries. For example, segregation measurements in samples from Magnox reactor control rods (4 wt% boron steel) irradiated at temperatures from 290 to 330 °C and to doses from 0.04 to 0.35 dpa, indicated that increasing Mo content reduced chromium depletion [49]. In the current EBR-II samples, however, greater grain boundary chromium depletion occurs in the sample with greater bulk molybdenum concentration, contrary to the Magnox measurements.

Examining Table 3, however, the differences in segregation do not correlate with any changes in bulk composition (there is no consistent change in bulk Fe, Cr, Ni, Mo, or Si moving from row 10 out to row 14 as there is with segregation. Bulk Mn does increase from row 10 to 14, but no experimental evidence is known showing that Mn composition strongly changes RIS). Since the differences in chromium depletion in the EBR-II materials do not correlate with differences in bulk composition, it is likely that they are caused primarily by the differences in dose rate.

Dumbill measured segregation in an Fe–18Cr–15Ni alloy irradiated with neutrons at 400 °C to 12.7 dpa in EBR-II [50]. The dose rate was not reported, but a typical experimental location in EBR-II had dose rates on the order of 10^{-6} dpa/s. The segregation measured by Dumbill is compared to the segregation measured in this study in Fig. 11. The segregation is larger in our lower dose rate samples. In the work by Dumbill, the Fe–18Cr–15Ni

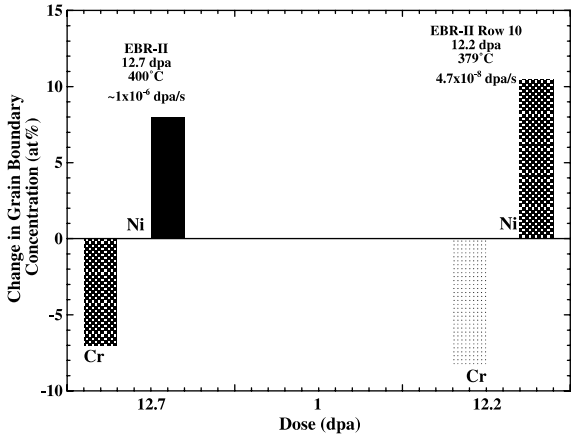

Fig. 11. Comparison of grain boundary segregation between inner row and outer row samples of 304 stainless steel irradiated in EBR-II. EBR-II inner row data from [50].

alloy has a greater bulk nickel concentration and therefore would be predicted to experience greater nickel enrichment and chromium depletion for similar irradiation conditions [51]. Additionally, at these relatively low temperatures, RIS increases as the temperature increases. Since the high dose rate samples show less segregation, even though they have greater bulk nickel concentration and were irradiated at higher temperature, the greater segregation in the EBR-II materials is most likely attributable to the difference in dose rate.

It should be noted, however, that the sample from row 14 was moved once during its lifetime, obtaining the last 7.6 of its total 10 dpa in row 14 after starting in row 10. Fig. 12 shows the calculated

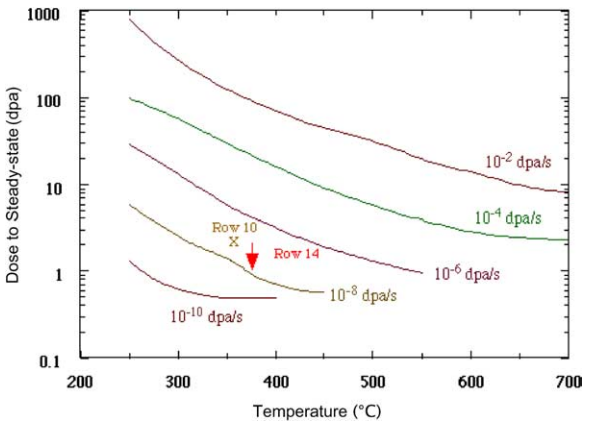

Fig. 12. Calculations indicate that even though the row 14 sample was moved once from rows 10 to 14 during its exposure, the RIS should have reached steady-state after 7.6 dpa in the final row 14 position.

time to steady-state RIS for different dose rates and temperatures [47]. For the row 14 dose rate of 2×10^{-8} dpa/s at 375 °C, RIS should reach steady-state by around 1–2 dpa. Since the row 14 sample received 7.6 dpa in position 14, it should be at steady-state and comparisons with row 12 and 10 samples are not likely to be affected by the sample movement.

Comparable to swelling, radiation-induced grain boundary chromium depletion and nickel enrichment in 304 stainless steel appear to increase at lower dose rate. Because data as a function of dose are not available at each displacement rate, the data presented here cannot discern if the greater segregation is due to a steady-state segregation difference or to a difference in the time to establish steady-state segregation profiles.

3.5. Tensile properties

Few studies have attempted to determine the effect of dose rate on mechanical properties. Modeling studies [52] as well as dislocation loop development studies in model alloys irradiated with neutrons and electrons [53] indicate that at constant temperature the dislocation loop density should increase with increasing damage rate. Since the yield strength varies with dislocation loop density and size, alloys may see damage rate-dependent changes in yield strength.

Brager et al. examined the effect of displacement rate on tensile properties of annealed Type 316 stainless steel [54]. For samples irradiated from 371 to 424 °C with a dose rate range of 0.8–8.4×10^{-7} dpa/s and tensile tested at 385 °C, no effect of dose rate on yield strength was noted. For samples examined in the TEM, microstructural features were significantly different between samples irradiated at 1.0×10^{-7} and 8.4×10^{-7} dpa/s to 3.3 dpa. The higher dose rate samples had a larger precipitate density while the lower rate samples had a higher void density. In the same study, an effect of dose rate on yield strength was noted for Type 304 stainless steel. Brager concluded that the lack of effect of dose rate on yield strength of Type 316 was a 'fortuitous situation in which a loss in strength contribution from precipitates as the displacement rate is decreased is offset by a concurrent gain in the strength contribution from the voids'.

A French study on solution annealed Type 316 stainless steel fuel cladding irradiated in the Rapsodie and Phenix reactors indicated that the saturation

yield stress was greater in material irradiated in Phenix. The material irradiated in Phenix was irradiated at twice the dose rate of material irradiated in Rapsodie [55].

Recently, Pokor et al. studied the tensile properties of annealed 304, 15% cold-worked 316, and Ti-modified 20% cold-worked 316 irradiated in the EBR-II, OSIRIS, and BOR-60 reactors [56,57]. The samples were irradiated at 330 °C in BOR-60 and at 375 °C in OSIRIS and EBR-II with tensile tests occurring at the same temperature as the irradiation. No obvious effect of dose rate or spectrum was noted as the yield strength increased as a function of irradiation dose.

The effect of displacement rate on yield strength and elongation can be examined by comparing 304 stainless steel samples irradiated in rows 4 and 12. Figs. 13 and 14 compare the yield strength and uniform elongation at 371 °C (also the irradiation temperature) for the row 12 (SURV) material and the row 4 (SURV) material. The yield strength of the row 12 cover plate material increases by about a factor of three over a dose of about 5 dpa. Even though the dose rate in row 4 is about an order of magnitude larger than that in row 12, the yield strength of the material irradiated in row 4 is generally similar to that irradiated in row 12. Superimposed on the row 4 and 12 data is a cubic curve fit, along with 95% confidence limits, to the row 12 data (a cubic relationship is not theoretically predicted, this curve is used only to help discern the data trends and the statistical variability in the data). No significant effect of displacement rate on dose rate on the yield strength is evident. Fig. 14 also indicates that no measurable effect is evident of displacement rate on uniform elongation.

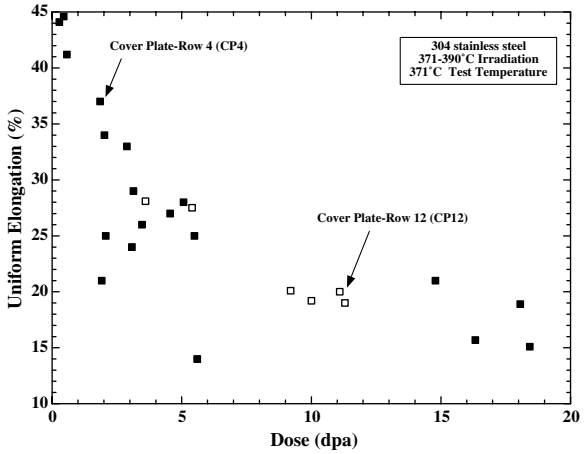

Fig. 14. Comparison of uniform elongation for 304 samples irradiated at different displacement rates.

The irradiation hardening can be examined by comparing the ratio of the yield strength (σ_y) to the ultimate tensile strength (σ_u) as a function of dose. As $1-\frac{\sigma_y}{\sigma_u}$ approaches zero, the material becomes harder. Fig. 15 plots $1-\frac{\sigma_y}{\sigma_u}$ for the row 12 cover plate material (CP12) tested at 371 °C, and the row 4 cover plate material (CP4) tested at 371 °C. The annealed cover plate material indeed hardens (the yield strength approaches the ultimate tensile strength) over the first 4 dpa and does not appear to depend on dose rate.

Tensile specimens from 12% cold-worked 316 hex ducts were also tested to investigate the effect of

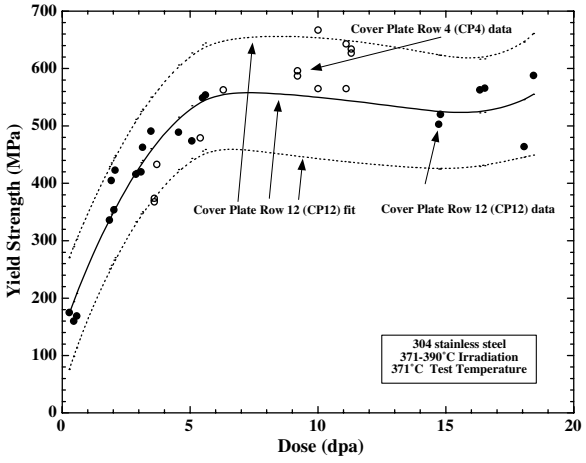

Fig. 13. Comparison of yield strength for 304 stainless steel samples irradiated at different displacement rates.

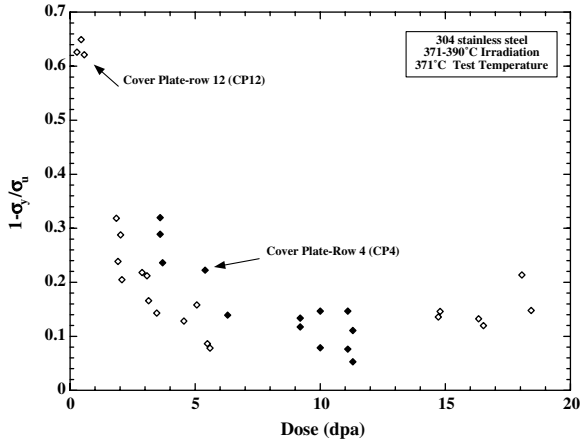

Fig. 15. Comparison of hardening for 304 samples irradiated at different displacement rates.

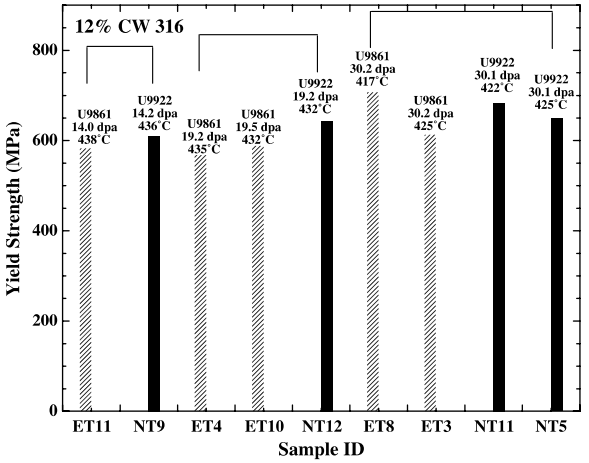

Fig. 16. Comparison of yield strength for 12% CW 316 samples irradiated at different dose rates. Row 8 (higher dose rate) samples have a designation that starts with E while row 9 (lower dose rate) samples have a designation that starts with N.

dose rate. The comparisons are shown in Fig. 16 for three groups of samples, each group irradiated at a similar temperature and dose. No strong trends of yield strength as a function of dose rate are seen. However, at lower doses (~14 and 19 dpa), the samples irradiated at lower dose rate have a higher strength. At higher dose (~30 dpa), no specific dose rate effect can be discerned. Although not shown, similar results (no dose rate effect) were seen in comparing the ultimate tensile strength and uniform elongation for 12% CW 316.

Examining the microstructural data from irradiated 12% CW 316 helps explain why no difference in tensile strength is noted for samples irradiated to the same dose at varying dose rates. The void and Frank loop size distributions were measured in 12% cold-worked 316 samples following irradiation. The average size along with the measured density is listed in Table 4 for two samples with irradiation temperature and dose comparable to the highest dose samples whose yield strength is reported in Fig. 16. These irradiation-induced defects are known to cause hardening. The hardening from each defect can be estimated from dispersed hardening theory [58]. The change in yield strength due to discrete obstacles is given by

$$\Delta\sigma_y = M\alpha\mu b\sqrt{Nd},$$

where M relates the shear stresses on a slip plane in a single crystal to the applied tensile stress necessary to activate slip in a polycrystal, α is the barrier strength, μ is the shear modulus of the matrix, b is the Burgers vector of a moving dislocation, N is the number density, and d the average diameter. The inverse of the quantity $\sqrt{Nd}$ represents average obstacle spacing.

The increment in yield strength due to loops and voids is typically calculated using a root-mean-square summation:

$$\Delta\sigma_y^{\text{voids+loops}} = \sqrt{(\Delta\sigma_y^{\text{voids}})^2 + \left(\Delta\sigma_y^{\text{loops}}\right)^2}.$$

The values of α and μ used to calculate the yield strength increment can be taken from Ref. [58] and are listed in Table 5. The values of M and b used to calculate the yield strength increment can be taken from Ref. [59] and are also listed in Table 5.

Calculating the ratio of the yield strength decrement from the data in Table 4 indicates the yield strength increase due to voids and loops would be roughly 20% higher at lower dose. Although the network dislocation density was not measured, the low dose samples were held at temperature twice as long as the high dose rate samples. The annealing of the cold work is expected to be greater in the low dose sample, mitigating the yield strength increase from the voids and loops. The difference in the measured yield strength between the high dose samples in Fig. 16 is roughly 15%. Therefore, the sample-to-sample variation in yield strength is as large as the microstructural component of the yield strength increase. The conclusion is that for the doses examined, the differences in microstructural development due to dose rate may be noticeable but do not contribute to a measurable difference in yield strength.

Table 4
Cavity and dislocation loop data for 12% CW 316

Dose rate (dpa/s)	Temperature (°C)	Dose (dpa)	Voids		Frank loops	
			Density (m^{-3})	Average diameter (nm)	Density (m^{-3})	Average diameter (nm)
4.2×10^{-7}	408	35.7	4.8×10^{21}	6.1	6.8×10^{21}	24.7
1.8×10^{-7}	414	35.7	2.6×10^{21}	8.8	8.2×10^{21}	32.9

Table 5
Constants for yield strength increment calculations

Parameter	Voids	Loops
M	3	3
α	1	0.33
μ	6.7×10^{10} Pa	6.7×10^{10} Pa
B	2.5×10^{-10} m	2.5×10^{-10} m

If a dose rate effect exists on tensile properties, it may only indicate at much larger doses or between much larger dose rate differences.

A final examination of the potential effect of dose rate on tensile properties was performed by comparing the yield strength, uniform elongation, and hardening of 20% cold-worked 316. Tensile tests were performed on samples taken from a row 8 hexagonal duct. The data were then compared with tensile data obtained by Fish from samples irradiated in row 2 in 1979 [60]. The comparisons are presented in Figs. 17–19. Note, however, that the materials irradiated in rows 2 and 8 did not come from the same heat of steel. The dose rate in row 2 is approximately one order of magnitude larger than that of row 8. To compare the two studies, the fluences reported by Fish were converted to doses using 2×10^{21} n/cm^2 ($E>0.1$ MeV) = 1 dpa.

The comparison of yield strength indicates that, even though both sets of data come from nominally 20% cold-worked Type 316 stainless steel, the row 8 material has a lower yield strength at 1 dpa than the unirradiated row 2 material. The yield strength for both sets of data increases as a function of dose similarly beyond 1 dpa. Because these ducts underwent standard quality assurance procedures prior to going into the reactor, the cold-work is not likely to differ significantly from the goal of 20%. On the other hand, the ducts from this study and that of Fish came from different lots of steel and the compositional differences may have caused a difference in unirradiated yield and ultimate tensile strength.

Table 6 compares the yield strength at low dose from three different experiments, the 20% cold-worked material irradiated in row 8 of EBR-II in this study, the 20% cold-worked material irradiated in row 2 of EBR-II in the Fish study, and 12% cold-worked material irradiated in row 9 of EBR-II in

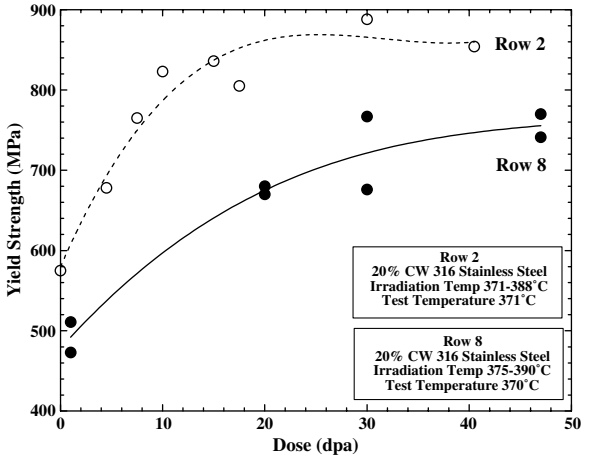

Fig. 17. Yield strength versus dose for 20% CW 316 samples irradiated in rows 8 and 2 EBR-II.

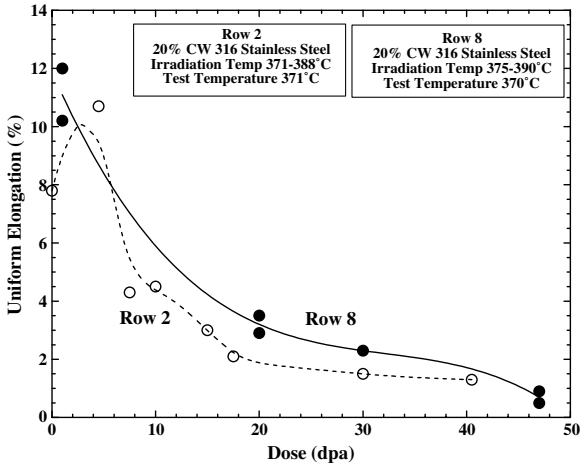

Fig. 18. Uniform elongation as a function of dose for 20% CW 316 samples irradiated in rows 8 and 2 of EBR-II.

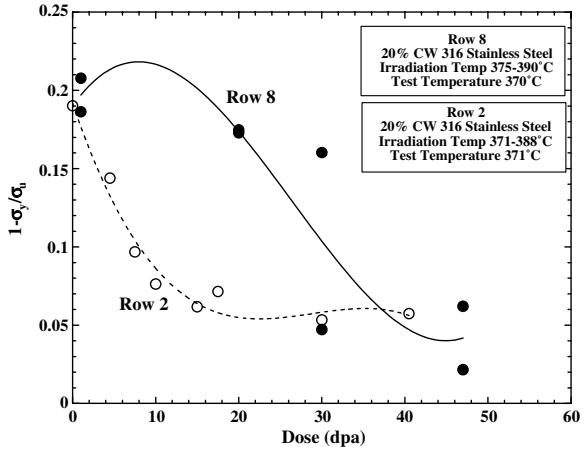

Fig. 19. Hardening as a function of dose for 20% CW 316. The higher dose rate row 2 samples lose work hardening capability faster.

Table 6
Effect of cold work on yield strength

Cold-work/irradiation position	Yield strength (370 °C) at low dpa (MPa)
12% Row 9 (this study)	~580 (1 dpa)
20% Row 8 (this study)	~500 (1 dpa)
20% Row 2 [60]	~575 (0 dpa)

this study. The difference between the largest and smallest yield strength in Table 6 is about 80 MPa.

Carson et al. measured the hardness at room temperature of Type 316 stainless steel as a function of cold-work [61] for various lots of material. For the material measured in Carson's study, the concentration of Cr varied from 16 to 18, Ni from 12 to 14, Fe from 64 to 69, and Mo from 2 to 3 wt%. For 12% cold-work, the room temperature hardness ranged from about 235 to 285 HV. Using the hardness-yield strength correlation developed by Higgy and Hammad [62], $\Delta\sigma_y = 3.27\Delta H_v$ to convert the hardness data of Carson et al. to yield strength, the range of yield strength as a function of composition is about 164 MPa. At 20% cold-work, the range of hardness converts to a range in yield strength of about 195 MPa. The difference in yield strengths noted in Table 4 is bounded by the hardness measured by Carson. Because of the large variability of strength with composition, a direct comparison of yield strength as a function of dose of the row 2 and 8 results cannot indicate if the irradiation dose rate has a significant effect on tensile properties.

The uniform elongation as a function of dose for the row 8 and 2 samples is plotted in Fig. 18. No significant difference in the uniform elongation is noted between the two data sets.

Fig. 19 displays the hardening $1 - \frac{\sigma_y}{\sigma_u}$ as a function of dose. The higher dose rate row 2 samples lose work hardening capability faster than the lower dose rate row 8 samples, even though there was no significant difference in the uniform elongation. Although no microstructural or fractography data are available from the Fish study, the loss of work hardening capacity may correspond with establishment of dislocation channeling as the primary deformation mechanism. If dislocations are free to travel through the material in slip bands, then less work hardening will occur. Fig. 20 compares the ratio of uniform to total elongation, using the same tensile tests from which the Fig. 19 data were taken. The ratio decreases more slowly for the row 2 higher

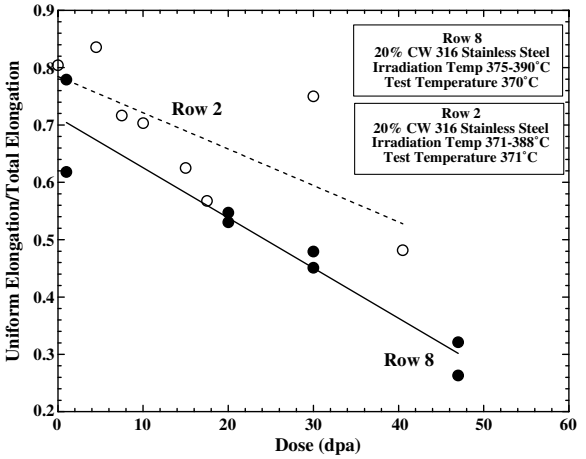

Fig. 20. Elongation ratios as a function of dose. The higher dose rate row 2 samples show greater post-yield necking.

dose rate samples. Since the uniform elongation was about the same for samples irradiated in rows 2 and 8 (Fig. 18), the difference lies in the total elongation. For the row 8 samples, greater necking occurs before the sample fails. Once again, it should be noted that the row 2 and row 8 samples were not from the same heat of steel so differences could be due to dose rate, but may also be due to compositional changes.

With the exception of the difference in the hardening in the 20% cold-worked 316 stainless steel, no systematic difference in tensile properties as a function of dose rate has been noted. The differences in swelling as a function of dose rate noted earlier are apparently not large enough to cause a notable effect on tensile properties, primarily because at these irradiation temperatures the void hardening is a small fraction of the total microstructural hardening.

4. Conclusions

Samples of 304 and 316 stainless steel were retrieved from EBR-II following shutdown. Density, tensile properties, and grain boundary segregation were measured with the goal of determining whether displacement rate has an appreciable effect on their radiation performance. Both swelling and RIS appear to be affected by dose rate, with greater swelling and greater grain boundary segregation occurring at lower dose rates. The trend was always seen, but was not always statistically significant, especially in CW 316 at low swelling levels and temperatures around 400 °C. The dose rate dependence

of swelling observed in these austenitic steels is consistent with a growing body of evidence showing similar behavior in a broad range of austenitic steels. For the range of dose rates examined, no discernable effect of dose rate on tensile properties was noticed. The lone exception was a difference in the rate the yield strength approached the ultimate tensile strength in 20% cold-worked 316 stainless steel. The hardening (rate at which the yield strength approached the ultimate tensile strength) occurred faster at higher dose rate. This hardening difference could also have been caused by compositional differences between two lots of 316 stainless steel. The measured difference in void development as a function of dose rate is apparently not large enough to cause a difference in tensile properties. The lack of strong dependence of tensile properties on dose rate insinuates that for the doses examined, surveillance data taken at different dose rates should be adequate for determining the properties of structural materials irradiated across different damage rates.

Acknowledgements

The authors gratefully acknowledge the efforts of M.E. Vaughn, J.P. Webb, E.L. Wood, and the staffs at the Hot Fuels Examination Facility at ANL-West. Thanks to K.A. Bunde for performing dose calculations and to R.T. Jensen for performing temperature calculations. Work supported at ANL under contract W-31-109-Eng-38 and at PNNL under contract DE-AC06-76RLO 1830 with the Department of Energy. Research at the Oak Ridge National Laboratory SHaRE User Facility was sponsored by the Division of Materials Sciences and Engineering, US Department of Energy under contract DE-AC05-00OR22725 with UT-Battelle, LLC. Portions of the work were supported by Mitsubishi Heavy Industries on behalf of a consortium of Japanese PWR utility groups. Funding for a portion of the studies came from the Japan Nuclear Cycle Development Institute. Funding for a portion of the studies came from the Central Research Institute of Electric Power Industry in Japan.

References

[1] IAEA-TECDOC-1119.
[2] A technology roadmap for generation IV nuclear energy systems, Report No. GIF002-00, 1 December 2002. Available from: <http://nuclear.gov>.
[3] F.A. Garner, in: Irradiation Performance of Cladding and Structural Steels in Liquid Metal ReactorsMaterials Science and Technology: A Comprehensive Treatment, vol. 10A, VCH Publishers, 1994, p. 419 (Chapter 6).
[4] F.A. Garner, L.R. Greenwood, D.L. Harrod, in: Proceedings of the Sixth International Symposium on Environmental Degradation of Materials in Nuclear Power Systems – Water Reactors, San Diego, CA, 1–5 August 1993, p. 783.
[5] F.A. Garner, Trans. Am. Nucl. Soc. 71 (1994) 190.
[6] F.A. Garner, M.B. Toloczko, J. Nucl. Mater. 251 (1997) 252.
[7] G.M. Bond, B.H. Sencer, F.A. Garner, M.L. Hamilton, T.R. Allen, D.L. Porter, in: 9th International Conference on Environmental Degradation of Materials in Nuclear Power Systems – Water Reactors, 1999, p. 1045.
[8] F.A. Garner, D.J. Edwards, S.M. Bruemmer, S.I. Porollo, Yu.V. Konobeev, V.S. Neustroev, V.K. Shamardin, A.V. Kozlov, in: Proceedings, Fontevraud 5, Contribution of Materials Investigation to the Resolution of Problems Encountered in Pressurized Water Reactors, 23–27 September 2002, paper #22, on CD format.
[9] V.S. Neustroev, V.K. Shamardin, Z.E. Ostrovsky, A.M. Pecherin, F.A. Garner, in: M.L. Hamilton, A.S. Kumar, S.T. Rosinski, M.L. Grossbeck (Eds.), Effects of Radiation on Materials: 19th International Symposium, ASTM STP 1366, American Society for Testing and Materials, 2000, p. 792.
[10] F.A. Garner, S.I. Porollo, A.N. Vorobjev, Yu.V. Konobeev, A.M. Dvoriashin, V.M. Krigan, N.I. Budylkin, E.G. Mironova, in: International Symposium on Contribution of Materials Investigation to the Resolution of Problems Encountered in Pressurized Water Reactors, Fontevraud, France, 14–18 September 1998, p. 249.
[11] S.I. Porollo, A.N. Vorobjev, Yu.V. Konobeev, A.M. Dvoriashin, F.A. Garner, in: International Symposium on Contribution of Materials Investigation to the Resolution of Problems Encountered in Pressurized Water Reactors, Fontevraud, France, 14–18 September 1998, p. 271.
[12] V.S. Neustroev, V.K. Shamardin, Z.E. Ostrovsky, A.M. Pecherin, F.A. Garner, in: International Symposium on Contribution of Materials Investigation to the Resolution of Problems Encountered in Pressurized Water Reactors, Fontevraud, France, 14–18 September 1998, p. 261.
[13] F.A. Garner, N.I. Budylkin, Yu.V. Konobeev, S.I. Porollo, V.S. Neustroev, V.K. Shamardin, A.V. Kozlov, in: 11th International Conference on Environmental Degradation of Materials in Nuclear Power Systems – Water Reactors, 2003, issued on CD format, p. 647.
[14] D.J. Edwards, E.P. Simonen, F.A. Garner, B.A. Garner, B.A. Oliver, S.M. Bruemmer, J. Nucl. Mater. 317 (2003) 32.
[15] V.S. Neustroev, Z.E. Ostrovsky, V.K. Shamardin, F.A. Garner, submitted for ATM 22nd Effects of Radiation on Materials, Boston, June 2004.
[16] N.I. Budylkin, T.M. Bulanova, E.G. Mironova, N.M. Mitrofanova, S.I. Porollo, V.M. Chernov, V.K. Shamardin, F.A. Garner, J. Nucl. Mater. 329–333 (2004) 621.
[17] S.I. Porollo, A.M. Dvoriashin, Yu.V. Konobeev, A.A. Ivanov, S.V. Shulepin, F.A. Garner, submitted for inclusion in Proceedings of ASTM Conference of Effects of Radiation on Materials, Boston, 2004.
[18] S. Greenberg, ANL-7624, September 1969.
[19] S. Greenberg, R.V. Strain, E.R. Ebersole, ANL-7682, June 1970.

[20] S. Greenberg, R.V. Strain, E.R. Ebersole, ANL-7937, September 1972.
[21] W.E. Ruther, G.O. Hayner, B.G. Carlson, E.R. Ebersole, T.R. Allen, ANL-98/3, January 1998.
[22] W.E. Ruther, J.D. Staffon, B.G. Carlson, T.R. Allen, ANL-98/4, March 1998.
[23] J.C. Van Duysen, P. Todeschini, G. Zacharie, in: A.S. Kumar, D.S. Gelles, R. Nanstad, E.A. Little (Eds.), Effects of Radiation on Materials: 16th International Symposium, ASTM STP 1175, American Society for Testing and Materials, Philadelphia, 1993, p. 747.
[24] T.R. Allen, C.L. Trybus, J.I. Cole, J. Nucl. Mater. 270 (1999) 290.
[25] G.L. Wire, in: D. Kramer, H.R. Brager, J.S. Perrin (Eds.), Effects of Radiation on Materials: Tenth Conference, ASTM STP 725, American Society for Testing and Materials, 1981, p. 375.
[26] F.A. Garner, J. Nucl. Mater. 122–123 (1984) 459.
[27] F.A. Garner, H.R. Brager, in: F.A. Garner, J.S. Perrin (Eds.), Effects of Radiation on Materials: Twelfth International Symposium, ASTM STP 870, ASTM, Philadelphia, PA, 1985, p. 187.
[28] F.A. Garner, D.S. Gelles, in: N.H. Packan, R.E. Stoller, A.S. Kumar (Eds.), Proceedings of Symposium on Effects of Radiation on Materials: 14th International Symposium, ASTM STP 1046, vol. II, American Society for Testing and Materials, Philadelphia, 1990, p. 673.
[29] F.A. Garner, D.L. Porter, in: Proceedings of International Conference on Dimensional Stability and Mechanical Behavior of Irradiated Metals and Alloys, Brighton, England, 11–13 April 1983, vol. II, p. 41.
[30] D.L. Porter, G.L. Hudman, Trans. Am. Nucl. Soc. 34 (1980) 230.
[31] D.L. Porter, F.A. Garner, in: F.A. Garner, J.S. Perrin (Eds.), Effects of Radiation on Materials: Twelfth International Symposium, ASTM STP 870, ASTM, Philadelphia, PA, 1985, p. 212.
[32] D.L. Porter, G.D. Hudman, F.A. Garner, J. Nucl. Mater. 179–181 (1991) 581.
[33] J.L. Seran, J.M. Dupouy, in: H.R. Brager, J.S. Perrin (Eds.), Effects of Radiation on Materials: Eleventh Conference, ASTM STP 782, American Society for Testing and Materials, 1982, p. 5.
[34] J.L. Seran, J.M. Dupouy, in: Proceedings of the Conference on Dimensional Stability and Mechanical Behavior of Irradiated Metals and Alloys, British Nuclear Energy Society, Brighton, London, vol. 1, p. 22.
[35] D.L. Porter, F.A. Garner, in: F.A. Garner, J.S. Perrin (Eds.), Effects of Radiation on Materials: 12th International Symposium, ASTM STP 870, American Society for Testing and Materials, Philadelphia, 1985, p. 212.
[36] H.R. Brager, F.A. Garner, in: Proceedings, International Symposium on Effect of Radiation on Structural Materials, ASTM STP 683, Richland, WA, 10–14 July 1978, p. 207.
[37] F.A. Garner, D.L. Porter, in: H.R. Brager, J.S. Perrin (Eds.), Effects of Radiation on Materials: Eleventh Conference, ASTM STP 782, American Society for Testing and Materials, 1982, p. 295.
[38] F.A. Garner, in: Proceedings of AIME Symposium on Irradiation Phase Stability, Pittsburgh, PA, 5–9 October 1980, p. 165.
[39] D.L. Porter, F.A. Garner, G.M. Bond, in: M.L. Hamilton, A.S. Kumar, S.T. Rosinski, M.L. Grossbeck (Eds.), Effects of Radiation on Materials: 19th International Symposium, ASTM STP 1366, American Society for Testing and Materials, 2000, p. 884.
[40] W.G. Wolfer, F.A. Garner, L.E. Thomas, in: H.R. Brager, J.S. Perrin (Eds.), Effects of Radiation on Materials: Eleventh Conference, ASTM STP 782, American Society for Testing and Materials, 1982, p. 1023.
[41] E.A. Kenik, Scr. Metall. 10 (1976) 733.
[42] E.A. Kenik, K. Hojou, J. Nucl. Mater. 191–194 (1992) 1331.
[43] T. Okita, N. Sekimura, F.A. Garner, L.R. Greenwood, W.G. Wolfer, Y. Isobe, in: 10th International Conference on Environmental Degradation of Materials in Nuclear Power Systems – Water Reactors, 2001, issued on CD format.
[44] T. Okita, N. Sekimura, T. Iwai, F.A. Garner, in: 10th International Conference on Environmental Degradation of Materials in Nuclear Power Systems – Water Reactors, 2001, issued on CD format.
[45] T. Okita, N. Sekimura, T. Sato, F.A. Garner, L.R. Greenwood, J. Nucl. Mater. 307–311 (2002) 322.
[46] T. Okita, W.G. Wolfer, T. Sato, N. Sekimura, F.A. Garne, in: 11th International Conference on Environmental Degradation of Materials in Nuclear Power Systems – Water Reactors, 2003, issued on CD format, p. 657.
[47] G.S. Was, T.R. Allen, J. Nucl. Mater 205 (1993) 332.
[48] F.A. Garner, T. Lauritzen, M.A. Mitchell, in: Proceedings of 16th ASTM International Symposium on Effects of Radiation on Materials, ASTM STP 1175, Denver, CO, 22–24 June 1992, p. 803.
[49] P. Spellward, J. Walmsley, R. Scowen, N. Partridge, J. Stump, R. Corcoran, T. Gilmour, V. Callen, in: Proceedings of the 8th International Symposium on Environmental Degradation of Materials in Nuclear Power Systems – Water Reactors, Amelia Island, Fl, August, American Nuclear Society, LaGrange Park, IL, 1997, p. 734.
[50] S. Dumbill, T.M. Williams, Proceedings of the Conference on Materials for Nuclear Reactor Core Applications, vol. 1, BNES, London, 1987, p. 119.
[51] T.R. Allen, J.T. Busby, G.S. Was, E.A. Kenik, J. Nucl. Mater. 255 (1998) 44.
[52] T. Hashimoto, N. Shigenaka, J. Nucl. Mater. 187 (1992) 161.
[53] T. Muroga, H. Watanabe, N. Yoshida, J. Nucl. Mater. 174 (1990) 282.
[54] H.R. Brager, L.D. Blackburn, D.L. Greenslade, J. Nucl. Mater. 122–123 (1984) 332.
[55] J.M. Dupouy, J. Erler, R. Huillery, in: Proceedings of the International Conference on Radiation Effects in Breeder Reactor Structural Materials, American Institute of Mining, Metallurgical, and Petroleum Engineers, 1977, p. 83.
[56] C. Pokor, Y. Brechet, P. Dubuisson, J.-P. Massoud, X. Averty, J. Nucl. Mater. 326 (2004) 30.
[57] C. Pokor, Y. Brechet, P. Dubuisson, J.-P. Massoud, A. Barbu, J. Nucl. Mater. 326 (2004) 19.
[58] G.E. Lucas, J. Nucl. Mater. 206 (1993) 287.
[59] F. Garner, M. Hamilton, N. Panayotou, G. Johnson, J. Nucl. Mater. 103–104 (1981) 803.
[60] R.L. Fish, N.S. Cannon, G.L. Wire, in: Effects of Radiation on Structural MaterialsASTM STP 683, American Society for Testing and Materials, 1979, p. 450.
[61] N.J. Carson Jr., C. Steves, C.J. Renken, K.J. Reinmann, H. Berger, ANL-7982, 1972.

[62] H.R. Higgy, F.H. Hammad, J. Nucl. Mater. 55 (1975) 177.
[63] T. Okita, T. Sato, N. Sekimura, F.A. Garner, L.R. Greenwood, W.G. Wolfer, Y. Isobe, in: Proceedings of the Tenth International Symposium on Environmental Degradation of Materials in Nuclear Power Systems-Water Reactors, National Association of Corrosion Engineers, Lake Tahoe, NV, 5–9 August 2001.
[64] D.B. Williams, C.B. Carter, in: Transmission Electron Microcopy: A Textbook for Materials Science, Plenum, New York, 1996, p. 321.